Atomization and Sprays, 19(1):1–15, 2009

MOLECULAR DYNAMICS SIMULATIONS OF NANODROPLET WETTING ON A SOLID SURFACE

N. Sedighi, S. Murad, and S. K. Aggarwal*
Department of Mechanical & Industrial Engineering,
Department of Chemical Engineering, University of Illinois at Chicago,
Chicago, IL 60607, USA

Original Manuscript Submitted: 7/23/07; Final Draft Received: 10/15/07

Surface wettability is of fundamental importance to myriad applications including many spray systems. It represents a multiscale phenomenon with scales ranging from continuum to molecular. In this paper, we report molecular dynamics (MD) simulations to investigate wetting characteristics of a nanodroplet on a solid surface. The shape of an initially spherical liquid droplet in contact with two solid surfaces has been studied by applying continuous pressure from two atomistic moving surfaces. An efficient algorithm has been developed to track the liquid-phase interface and the dynamic contact angle θ, and characterize the wetting properties under the forced spreading of a droplet on a surface. Using a relatively small number of atoms (on the order of 10^4), the algorithm has been demonstrated to reproduce the entire wetting regime $0^o < \theta < 180^o$ by varying the solid–liquid interaction energy. Extensive simulations have been performed to investigate the effects of changes in surface and liquid droplet characteristics on the wetting phenomena and contact angle. Results indicate a highly complex relationship between the contact angle and many surface and liquid characterizing parameters. The present study clearly demonstrates that MD simulations can be effectively used for a fundamental investigation of the wetting phenomena under forced spreading, and for characterizing the effects of surface tension and other macroscopic properties on wettability by suitably changing the liquid and surfaces molecular parameters.

INTRODUCTION

Wetting of surfaces is of critical importance in many diverse areas of fundamental and applied sciences. Surface wettability is important in controlling many important industrial processes, including soldering, brazing, coating, and composite processing. Wetting and interfacial forces are responsible for the behavior of commonly used materials such as paints, adhesives, detergents, and lubricants. Self (spontaneous) and forced droplet spreading on a surface are important to myriad existing and emerging technologies, including spray combustion systems, material synthesis, and microelectronics. In many recent studies of microfluidics and nanosystems, droplet wetting has been shown to play an important role [1]. Surface wetting is also an important consideration in agricultural sprays and the application of pesticides.

Wetting is commonly characterized by the contact angle θ, which is defined as the angle where the liquid–gas interface contacts the solid surface, or the angle subtended between liquid–vapor and the liquid–solid interfaces. The contact angle indicates the degree of wetting. The lower the contact angle, the greater is the wetting. The dynamics of the wetting or spreading process is described by the variation of the instantaneous contact angle with time or contact line (wetting) velocity. The usual description of surface wetting under ideal conditions is based on Young's equation [2], which relates the equilibrium or static contact angle θ to the surface tension of the interfaces, and is given by

*Corresponding author; e-mail: ska@uic.edu. SM was partially supported by NSF Grant No. CTS-0730026.

1044–5110/09/$35.00

$$\gamma_{lv} \cos \theta = (\gamma_{sv} - \gamma_{sl}) \quad (1)$$

Here, γ is the surface tension or surface energy per unit area of the interface, and *s*, *l*, *v*, represent solid, liquid, and vapor, respectively. In actual experiments, the contact angle depends on additional factors such as the static and dynamic conditions, chemical heterogeneity, surface roughness, swelling of the solid by the liquid, and chemical reactions. For example, surface heterogeneity and/or roughness could well cause variations of the contact angle along the three-phase contact line. The existence of these effects is well known, but has not been investigated systematically. Many other theoretical approaches based on Young's equation have also been developed to account for other nonideal contributions. However, direct experimental verification of Young's equation is still lacking [3]. Moreover, despite its success in offering practical insight into the wettability and spreading phenomena, this equation has been the subject of considerable controversy and debate.

Due to its diverse applications and fundamental importance, the phenomenon of surface wetting has been extensively investigated from different aspects. While Young [2] and Laplace [4] reported pioneering work dealing with the theoretical aspects of the contact angle in the early nineteenth century, more systematic research on the wetting phenomena started in the 1960s. A thermodynamic analysis of surface wettability was reported by Zisman [5], Fowkes [6], and Padday [7]. Studies on the dynamics of liquid spreading started with the pioneering work of Huh and Scrivan [8]. Heslot et al. [9] and Sikalo et al. [10] experimentally investigated the dynamics of spreading by considering the impact of a droplet on a substrate. They observed that the existing empirical models do not predict the experimentally observed changes in the dynamic contact angle, especially at high capillary numbers ($C_a = \mu V/\gamma$; here μ is the viscosity of the liquid, V is the spreading velocity of the contact line, and γ is the liquid surface tension).

Ruijter et al. [11] investigated the spontaneous spreading of a liquid using molecular modeling, while Cheng and Ebner [12] performed two-dimensional Monte Carlo simulations to study the dynamics of spreading under wetting and nonwetting conditions. Thompson [13] used molecular dynamics (MD) simulation to study two immiscible fluids confined in a Couette geometry to determine the dynamic contact angle and contact line as functions of shear rate. Koplik et al. [14] also performed MD simulations to study low Reynolds number flow of a Lennard-Jones fluid in a channel. They found that the static contact angle for an immiscible two-fluid system was predictable, and varied with flow velocity for an accelerating flow. Fukai et al. [15] reported a theoretical and experimental study on the deformation of a droplet colliding with a flat surface, and observed that the maximum spreading radius decreases as the advancing contact angle increases. Joanny and de Gennes [16] investigated the dynamics of the contact angle and observed the presence of hysteresis in the contact line for strongly heterogeneous surfaces. Muller et al. [17] found a strong correlation between the surface roughness and wetting behavior of a solid. The transition from complete wetting to partial wetting was first predicted by Cahn [18]. Lenz and Lipowsky [19] studied the morphological transitions of wetting layers on imprinted surfaces, and observed that a droplet in a single domain exhibits a contact angle that does not satisfy Young's equation. Nijmeijer et al. [20] performed MD simulations of a liquid slab confined between two surfaces in order to examine the transition from a partially wet to completely wet and from a partially dry to completely dry surface. Maruyama et al. [21] performed MD simulations to study the microscopic aspects of the liquid–solid contact phenomena and phase-change heat transfer. Klier et al. [22] measured the contact angle (θ) of super liquid 4He on a cesium-coated tungsten plate as a function of temperature, and found that θ decreases to zero at $T \approx 2$ K. Werder et al. [1] studied the behavior of a water droplet in a carbon nanotube using MD simulations, and reported contact angles for tube radii ranging from 12.5 to 37.5 Å. Verheijen and Prins [23] measured the contact angle of a droplet by measuring the capacitance between a conducting droplet and a subsurface counter electrode. Fan and Cagin [24] performed MD simulations to study the wetting of polymer surfaces, and computed the contact angle from the droplet volume and the interfacial area between the droplet and the surface.

The wetting phenomenon involves scales ranging from continuum to molecular, and has thus been described in terms of both the hydrodynamic [25] and molecular theories [26]. At the continuum level, the droplet spreading is generally described in terms of inertial (in the case of forced spreading), capillary, and viscous forces. Accordingly, the continuum-based experimental [27, 28], theoretical [29, 30], and numerical [31] investigations have examined droplet spreading in terms of the Weber number, capillary number, and Reynolds number. For instance, the spreading characteristics, such as spreading radius, contact angle (both dynamic and equilibrium), and contact line speed, have been obtained in terms of the appropriate nondimensional parameters. The wetting phenomenon has also been described in terms of molecular processes [1, 11, 13, 32], which play a fundamental role in determining the fluid–solid interactions, dynamic contact angle, and singularity at the moving contact line. Moreover, the global wetting behavior can also be described in terms of molecular dynamics. For instance, at the liquid-solid interface, if the liquid molecules have a stronger interaction with the molecules that constitute the solid surface than to each other (i.e., if the adhesive forces are stronger than the cohesive forces), then wetting of the surface occurs. Alternatively, if the liquid molecules are more strongly attracted to each other, and not to the molecules of the solid surface (the cohesive forces are stronger than the adhesive forces), then the liquid beads up and does not wet the surface.

The literature review indicates that the wetting phenomena associated with a droplet in contact with a solid surface has been extensively investigated experimentally, theoretically, and numerically. While the experimental and theoretical studies have considered macrosize droplets and examined hydrodynamic aspects of wetting, the numerical studies have employed both macrosize and nanosize droplets using continuum and MD simulations, respectively. With regard to the latter, most previous studies have considered a droplet placed on a surface, and examined the dynamics of wetting as this initially spherical droplet equilibrates to a shape determined by the droplet and surface properties. In the present investigation, we employ a rather novel configuration to simulate the dynamics of forced spreading of a nanodroplet on a surface. The configuration involves an initially spherical nanosize droplet that is squeezed between two surfaces that move in the opposite directions. This type of wetting is expected to play an important role in the design and operation of nanomachines and nanolubrication. Moreover, this approach has allowed us to reach the equilibrium state much faster than previous studies. In most of our simulations, equilibrium was reached in about 20,000 time steps, while previous simulations required numbers of time steps that were typically an order of magnitude higher [11]. Our algorithm also allowed us to have two solid–liquid interfaces, which permitted us to effectively have two independent contact angles within a single simulation, leading to better accuracy. We have been able to examine the entire wettability regime ranging from $\theta \to 0$ to $\theta \to 180$ deg by changing the surface-liquid parameters. In addition, using detailed numerical experiments, it has been demonstrated that this configuration is quite effective for a fundamental investigation of the dynamics of wetting under forced spreading, and for characterizing the effects of surface tension and other macroscopic properties on wettability by suitably changing the liquid and surface molecular parameters.

MD SIMULATION MODEL

Previous investigations by others and us [33] have demonstrated that molecular dynamics simulation is one of the most powerful techniques to investigate droplet dynamics and related behavior. In the MD simulation, specifying the total number of particles and the initial average number density for the simulated system yields the overall system volume, which in the present investigation is the rectangular cube illustrated in Fig. 1. The dimensions of the simulation system are $L_x = 69.88\sigma$, $L_y = 34.94\sigma$, and $L_z = 34.94\sigma$, which are approximately equal to $L_x \approx 24$ nm, $L_y \approx 12$ nm, and $L_z \approx 12$ nm. Here σ is the characteristic length scale, and represented by the Lennard-Jones (LJ) diameter of argon atom in our simulation.

All the atoms are initially placed at the lattice site of a face-centered cube (FCC) in the simula-

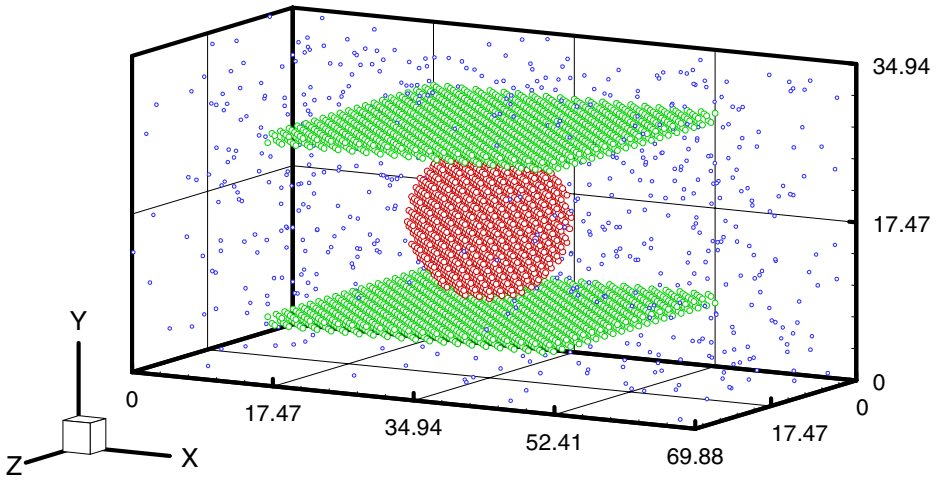

Fig. 1 Simulation system containing a liquid droplet placed between two parallel solid surfaces and ambient gas atoms. For clarity, the ambient gas atoms are shown smaller than actual size.

tion system. The density and initial temperature of the system were specified to correspond to the state condition being investigated. The droplet is then formed by removing all the atoms not falling within the boundaries of the droplet, which is centered at $(x, y, z) = (L_x/2, L_y/2, L_z/2)$ with a radius of $L_y/4$. This results in a droplet containing 2123 Lennard–Jones (LJ) particles for the present study. The region outside the droplet was then filled with the ambient gas atoms, with its density corresponding to the desired partial pressure. This yields 976 atoms representing the ambient gas. The simulation system thus contains 6379 (N_t) argon atoms, of which 2123 (N_f) atoms constitute the droplet, 3280 (N_w) atoms constitute the two surfaces, and 976 (N_a) atoms constitute the ambient gas. The fluid particles can move freely in the 3D system, as determined by the prescribed potential energy equation. In order to simulate a physically realistic system, periodic boundary conditions are employed at the system boundaries.

The liquid droplet is initially placed between two atomistic surfaces parallel to the x–z plane. Each surface consists of two layers of atoms forming two planes of fcc lattice, as shown in Fig. 1. The droplet initially has a spherical shape with a diameter $d = 17.47\sigma$, or ~6.0 nm, which is equal to $L_y/2$. The droplet is located at the center of the two solid surfaces, i.e., the solid surfaces are initially tangent to the droplet surface. The droplet is then squeezed slowly between the surfaces by moving the surfaces at a constant speed V in opposite directions along the y-axis. The surrounding vapor or ambient gas has an initial density of $\rho_a = 0.0167\rho_f$.

Interactions between the fluids' atoms were modeled using the Lennard-Jones (LJ) potential.

$$U_{ij}(r) = 4\varepsilon_{ij}\left[\left(\frac{\sigma_{ij}}{r}\right)^{12} - \left(\frac{\sigma_{ij}}{r}\right)^{6}\right] \qquad (2)$$

Here ε and σ are characteristic energy and size parameters, respectively, and r is the center–center distance. For argon atoms, $\varepsilon = 1.67 \times 10^{-21}$ J, and σ = 3.405 Å. In order to improve the computational efficiency, the potential was truncated at a cutoff distance of 3σ. The validity of this approach has been demonstrated in several previous studies [11, 14]. The simulation details for the first set of simulations are as follows. The fluid density and initial temperature are $0.75\sigma^{-3}$ and $0.72\varepsilon/k$, respectively. The surface-surface interactions were also modeled with the LJ potential. To maintain a well-defined solid structure, each surface atom was attached to its lattice site with a simple harmonic potential, with a spring constant of $K = 200\varepsilon/\sigma^{-2}$, and was allowed to oscillate due to thermal fluctuations around its lattice position. For the refer-

Table 1 Parameters Used for Different Sets of Simulations

Case	ε_f	ε_w	σ_f	σ_w	ρ_f	ρ_w	d
1 (Reference)	1.0	1.5-0.01	1.0	1.0	0.75	0.75	$0.5d_i$
2	1.0	1.5–0.01	0.9	1.0	0.56	0.75	$0.5d_i$
3	1.0	1.5–0.01	1.0	0.9	0.75	0.56	$0.5d_i$
4	0.75	1.5–0.01	1.0	1.0	0.75	0.75	$0.5d_i$
5	1.0	1.5–0.01	1.0	1.0	0.75	0.75	$0.4d_i$

ence case, we used $\rho_w = 0.75\sigma^{-3}$. The dimensions of the two surfaces were initially taken as one-half of the system size in the x direction ($L_{x\text{–surface}} = L_x/2$), and equal to the system size in the z direction ($L_{z\text{–surface}} = L_z$). Each surface consisted of two layers of atoms, which corresponds to a thickness of 0.64 nm. The initial distance between the surfaces is 17.47σ, or one-half of the system size in the y direction, while the final distance is one-half of the initial distance, or one-fourth of the cube size in the y direction. The tethering sites of the atoms are then moved, which then drag the atoms constituting the surfaces, while they are allowed to fluctuate to ensure thermal equilibrium.

The initial velocities of all system particles are assigned randomly as the Gaussian distribution based on the desired initial temperature. During equilibration, the system temperature is kept constant and a well-defined droplet is formed. The end of the initialization period corresponds to the start of the production part of the simulation, and therefore represents the origin of time for the results reported here.

The equations of motion were integrated using Gear's fifth-order predictor–corrector algorithm. The time step is $\Delta t = 0.05\tau$ (1.078×10^{-2} ps), where $\tau = (m\sigma^2/\varepsilon)^{1/2}$ with m being the mass of an argon atom. The reduced initial temperature is $T^* = kT/\varepsilon = 0.72$. The porosity of the moving surfaces was fixed to prevent any diffusion of atoms across the solid surfaces. The system was equilibrated for ~500 time steps before the surfaces began to move. The coordinates of all molecules were subsequently sampled every 500 steps for later analysis. The two surfaces move toward each other with a constant speed of $V = 0.218 \times 10^{-3}\sigma$ per time step, or ~7.0 m/s.

Numerical experiments were conducted with several values of Δt to assure that the simulations are reasonably independent of the time step. In addition, in order to further validate our results we performed simulations with surfaces larger than those described earlier. The results for surfaces with dimensions of $L_x \times L_z$ were in agreement with those of size $L_x/2 \times L_z$. All the simulations were therefore carried out with a smaller surface in order to reduce computational time.

Several sets of MD simulations were performed to determine the effects of droplet and surface parameters on the contact angle and wetting properties (see Table 1). The first set of simulations focused on observing the dynamics of droplet wetting and contact angle with the solid surface by moving the surfaces at a fixed velocity as discussed earlier. An algorithm[1] was developed to track the interface based on the computed density profiles, and thereby determine the contact angle. Subsequently, the variation of contact angle with the liquid–surface interaction parameters was quantified.

In the second set of simulations, the liquid molecular diameter (σ_f) was changed, while keeping the rest of the simulation parameters fixed. Note that a reduction in σ_f decreases the liquid–liquid interactions relative to the liquid–surface interactions, since the intermolecular distance between liquid particles is effectively increased. In the third set of simulations, the effect of surface porosity on droplet wetting and contact angle was investigated by changing the diameter of the solid particles (σ_w). By reducing σ_w, the porosity was increased while the droplet–

[1]This algorithm is described in the next section.

surface interaction was decreased. In the fourth set, the effect of the liquid–liquid interaction energy parameter (σ_f) on the contact angle was investigated. By reducing σ_f, the effective liquid–surface interaction is enhanced relative to the liquid–liquid interaction. Another set of simulations was performed to investigate the effect of the extent of droplet compression on the contact angle. For this purpose, the final distance between the surfaces was reduced further, while keeping other parameters unchanged. The results indicated no significant change in droplet–surface interactions, providing another validation of our simulations.

Theoretical studies show that the nature of the solid–liquid interface is determined by the competition between solid–liquid and liquid–liquid interaction forces. Due to the presence of two surfaces, there are two solid–fluid interfaces in our simulations. In our approach, moving the surfaces instead of the droplet assures even spreading of the droplet on the solid surface, leading to, as mentioned earlier, a much more efficient simulation. The liquid surface under the effect of unbalanced forces on its interfacial molecules behaves like a stretched membrane characterized by the surface or interfacial tension γ. It is well known that it is necessary to supply energy to create this surface. This energy is known as the surface free energy. In the case of two fluid interfaces, this energy is defined by the work done against the surface tension in expanding an interface to create a new area of interface [34].

$$\delta W = \gamma dA \tag{3}$$

For an interface that is bounded at least on one side by a solid, the above definition of surface free energy may not necessarily be true. As discussed by Woodruff [35], an alternate way is to assume that a crystal consists of atoms interacting attractively in pairs by means of forces of finite range, and then the surface energy is given by the sum of the energies of all bonds broken by the surface and passing through unit area of the surface. The free surface energy is then given by

$$F = U - TS \tag{4}$$

where U is the internal energy, T the absolute temperature, and S the entropy. Using the assumption of constant temperature and employing the first and second laws of thermodynamics yields $dF = PdV$. Since PdV represent the work done on the system, the definition of free surface energy for any closed surface leads to Eq. 3, which can be integrated to yield

$$F = \int \gamma(n)\, dA \tag{5}$$

Here n is outward normal to the elemental surface dA. The thermodynamic equilibrium is reached when the shape corresponds to the minimum value of F. In the present study, we have examined both the equilibrium and dynamic wetting characteristics.

RESULTS AND DISCUSSION

For the results reported in this paper, all variables are reduced with argon parameters reported earlier ($\varepsilon = 1.67 \times 10^{-21}$ J, $\sigma = 3.405$ Å, and m = 39.948 amu). In the first set of simulations, which is referred to as the reference set, the reduced σ for the surface and droplet atoms have the same value, i.e., $\sigma_w = \sigma_f = 1$, and $\varepsilon_f = 1$. Table 1 lists the values of various parameters used in our simulation.

The wetting properties of the system were then investigated by varying the energy parameter ε_w of the surface, which affects the surface–liquid interaction via the mixing rule, $\varepsilon_{ij} = (\varepsilon_i \varepsilon_j)^{1/2}$. The dynamics of the wetting process for two rather extreme values of ε_w is depicted in Fig. 2, which presents instantaneous two-dimensional (x–y) snapshots of all particle positions (droplet and the two surfaces) at four different instants during the simulation, corresponding to wettable (ε_w = 1.0) and nonwettable (ε_w = 0.01) surfaces. As the two surfaces move toward each other, the droplet between them is squeezed and the interface assumes a spheroidal shape to satisfy the minimum energy requirement. As the droplet is squeezed further due to the movement of the surfaces, its surface (interface between the droplet and ambient gas) assumes a concave or a convex shape corresponding to a hydrophilic (wettable) or hydrophobic (nonwettable) surface, respectively. After 20,000 time steps, the system was allowed to fur-

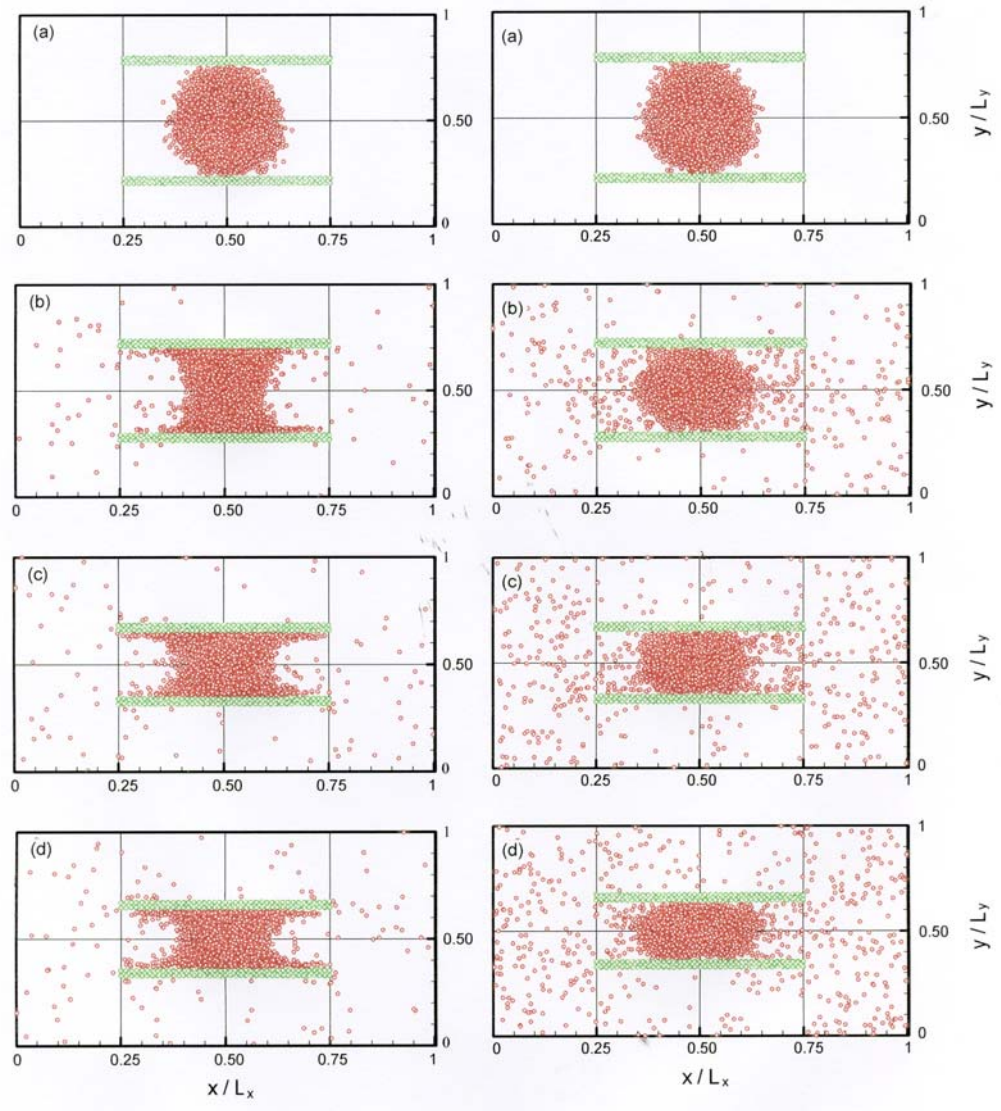

Fig. 2 Instantaneous 2D snapshots (x–y view) of particle positions at time (a) $t = 10\Delta t$, (b) $t = 10{,}000\Delta t$, (c) $t = 18{,}000\Delta t$, (d) $t = 25{,}000\Delta t$. Where $\Delta t = 1.078 \times 10^{-14}$ s. Snapshots indicate the dynamics of the surface wetting as the droplet is squeezed by moving the surfaces for two cases: ε_w = 1.0 (hydrophilic surface) and 0.01 (hydrophobic surface).

ther equilibrate while the two surfaces remained stationary. Such equilibrium was reached in about 5000 steps.

The contact angle (θ) of the interface between solid, liquid, and vapor can be determined by measuring the slope of the curve passing through the interface. Depending on the strength of the interaction between solid and liquid (i.e., the magnitude of ε_w), the contact angle can vary from 0 to 180 deg, with the former corresponding to high energy of interaction between the solid and liquid and resulting in complete wetting. The four images on the left of Fig. 2 for ε_w = 1.0 correspond to a relatively high wetting surface. As ε_w is reduced, the surface–liquid interaction decreases and the contact angle thereby increases. For contact angles between $0 < \theta < \pi/2$, the surface is characterized as hydrophilic or wettable. As ε_w is reduced further, interaction between the liquid atoms becomes stronger than that between the liquid and surface atoms, and the contact area between fluid and surface therefore decreases. In this case, the contact angle becomes greater than $\theta > \pi/2$ and the surface is charac-

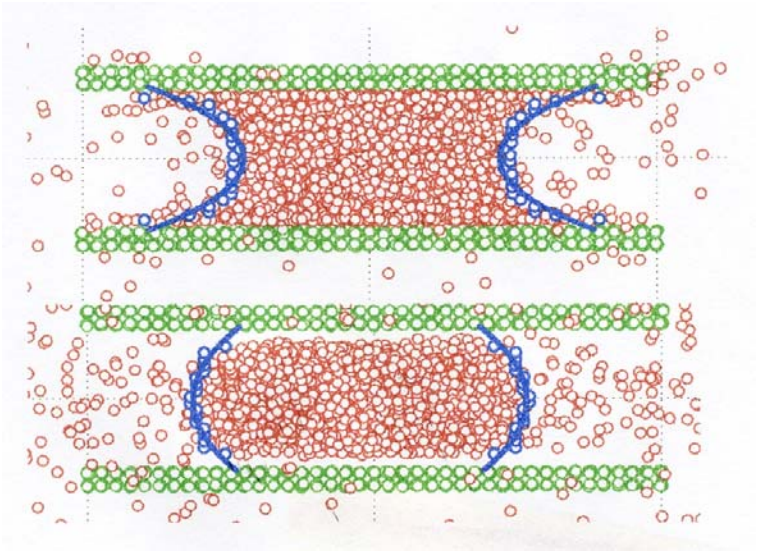

Fig. 3 Average positions of the droplet atoms and the data points showing the liquid–vapor interface and contact angle for hydrophilic (ε_w = 1.0) and hydrophobic ε_w = 0.01) surfaces.

terized as partially wettable, and as ε_w is reduced further, θ becomes closer to 180 deg, and the surface is characterized as nonwettable or hydrophobic. The four images on the right of Fig. 2 for ε_w = 0.01 correspond to a nonwettable surface. Therefore, the results in Fig. 2 clearly illustrate that our MD simulation scheme can reproduce the entire wettability regime under forced wetting by suitably changing ε_w. Figure 2 also indicates considerably more evaporation for ε_w = 0.01 compared to that for ε_w = 1.0. A weaker interaction with the surface shifts the phase equilibrium and a higher vapor pressure is necessary for equilibrium, resulting in more evaporation for the former case. This is because the decreased interaction between the droplet and the surface effectively decreases the system critical temperature, which leads to higher vapor pressure for the system.

Computation of Contact Angle

In order to quantify the effects of various surface and liquid properties on the wetting characteristics, an algorithm was developed to determine the contact angle using the computed density profiles. For this analysis, the simulation system was divided into a large number of 3D parallelepiped bins with 40 and 80 bins in the x and y directions, respectively. Therefore, each bin volume is $(L_x/40)\,(L_y/80)L_z$. The interface was determined by identifying the bins that belong to the droplet surface. The positions of the atoms were monitored during the last 5000 steps of the simulation (when the droplet was relatively stationary). The average density profiles were computed by counting the number of particles in each bin. The bins were examined for this analysis by traversing the system box systematically along the x direction (in the x–z plane), starting from the bottom surface. The liquid–vapor interface was then determined by comparing the density in each bin with the density in the core bin (at the center of the droplet) in each x–z plane, and defining the interface at the position where ρ_{bin} is reduced to $\leq 0.2\rho_{core}$. Considering the system symmetry with respect to the y–z plane (at $x = L_x/2$) and x–z plane (at $y = L_y/2$), the interface thus obtained was then smoothed by fitting a single curve through the interface bins of both solid–liquid surfaces. The contact angle, which is the angle of intersection between the surface of the droplet and the surface, was obtained by determining the slope of the interface curve at $y = y_{wall}$. Figure 3 shows plots for the computed interface and the contact angle for the typical wettable and nonwettable surfaces. The contact angle reported in this paper (cf. Fig. 4) was taken as the average of the four contact angles between the liquid and solid, as indicated in

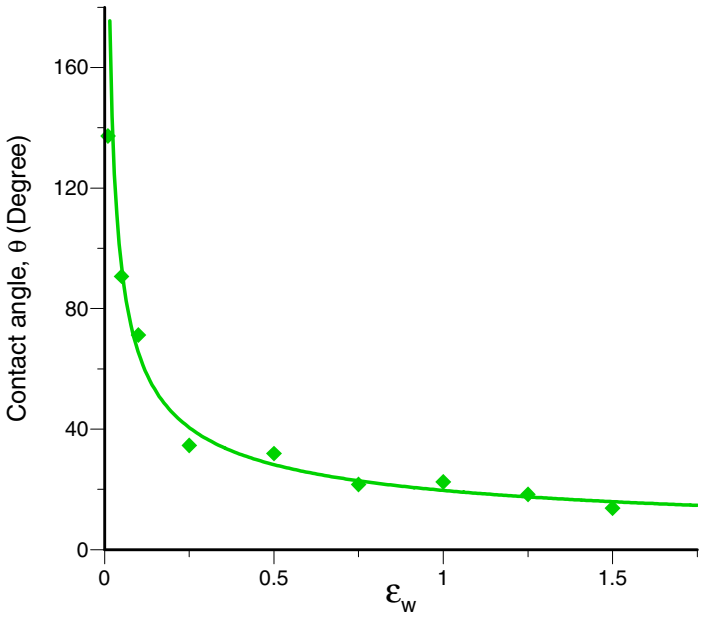

Fig. 4 Plot of contact angle as a function of the surface–liquid interaction energy parameter (ε_w) for the reference case.

Fig. 3. This further improves the accuracy of the computed results. The equilibrium contact angles computed using this procedure are 22.5 deg and 137.3 deg, respectively, for the wettable (ε_w = 1.0) and nonwettable (ε_w = 0.01) surfaces depicted in Fig. 3.

Effect of Surface–Liquid Interaction Energy Parameter (ε_{wf})

The surface wetting characteristics were then investigated by performing simulations with the reference parameter set (see Table 1) for values of ε_w ranging from 1.5 to 0.01, and computing the wetting dynamics and contact angle. Figure 4 presents the contact angle plotted as a function of ε_w. The contact angle is observed to vary from θ = 12.78 deg to θ = 137.3 deg, as ε_w is varied from 1.5 to 0.01. The corresponding range for ε_{wf} is 1.224 to 0.1. The maximum uncertainty in the computed contact values is 10%. For ε_w = 1.5, simulations indicate a relatively large wetting surface, since there is high degree of interaction between droplet and surface, and the droplet spreads over a large area and the contact angle is small. As ε_w is decreased from 1.5 to 0.01, the droplet wetting or spreading area on the surface becomes smaller, and the contact angle increases. For $\varepsilon_w < 0.1$, the contact angle becomes greater than $\pi/2$, i.e., the slope of the interface becomes negative, and the wetting characteristics change from a wettable to a nonwettable surface. For ε_w = 0.01, the contact angle θ = 137.3 deg indicates a highly nonwettable or hydrophobic surface. Figure 4 further indicates that the contact angle would vary from θ = 0 (completely wettable) to $\theta = \pi$ (completely nonwettable surface) if ε_w is varied from ∞ to 0. In addition, it is observed that the relationship between the contact angle and surface interaction energy ε_w is highly nonlinear. For $\varepsilon_w < 0.1$, the contact angle changes quite rapidly with ε_w, while for $\varepsilon_w > 0.1$, the rate of change of θ becomes relatively small. This also explains the large variation in wetting characteristics observed in materials with rather similar structures. These results qualitatively agree with previous theoretical and experimental studies. During the simulation, it was also observed that vaporization could affect the contact angle dynamics. Vaporization results in a fuzzy interface, which results in some uncertainty in determining the contact angle. Indeed, the high rate of vaporization and the nonisothermal nature of the vapor–liquid interface can generate variation in surface tension that eventually leads to the instability of the contact line. However, this aspect

was not examined in the present study.

Effect of Droplet Compression on Contact Angle

Simulations were also performed to examine the sensitivity of the computed contact angle to the degree of droplet compression by the two surfaces. For this purpose, the surfaces were allowed to continue their motion toward each other until the distance between them reached 40% of the original distance (50% in the reference case). Figure 5 presents the variation of contact angle with ε_w for two different values of the final distance. Results indicate that the wetting characteristics are relatively insensitive to the amount of droplet squeezing. This provides further validation of our numerical algorithm.

Effect of Liquid Molecular Diameter (σ_f)

The preceding simulations have clearly demonstrated the feasibility of our approach for examining the wetting dynamics and contact angle associated with the forced spreading of a droplet on a surface. We now present a series of simulations to characterize the effects of various liquid and solid properties on the contact angle. In the next set of simulations, the effect of droplet molecular diameter (σ_f) on the contact angle is investigated by changing σ_f from 1.0 to 0.9. Even with the smaller σ_f, we ensured that no diffusion occurred across the surfaces. All other parameters of the system are kept unchanged. The surface-liquid interaction energy parameter ε_w is again varied from 1.5 to 0.01. Figure 6a shows the variation in the contact angle with respect to ε_w for $\sigma_f = 0.9$ and 1.0. For $\varepsilon_w < 0.2$ (corresponding to a nonwettable surface), the contact angle values are nearly the same (within our error bars) for the two cases, while for $\varepsilon_w > 0.2$ (corresponding to a wetting surface), the contact angle decreases, i.e., the wettability increases as the droplet molecular diameter is decreased. This is because reducing σ_f effectively increases the interatomic distance between the droplet molecules (relative to the size of the molecules), making the cohesive forces weaker relative to the adhesive forces, and thereby decreasing the contact angle. It is interesting to note, however, that this effect is only noticeable in the wetting regime.

Effect of Surface Porosity (σ_w)

The effect of surface porosity was investigated by changing the molecular diameter of the atoms constituting the surfaces. By decreasing σ_w from 1 to 0.9, the porosity of the surface increased from 0.75 to 0.85. All other simulation parame-

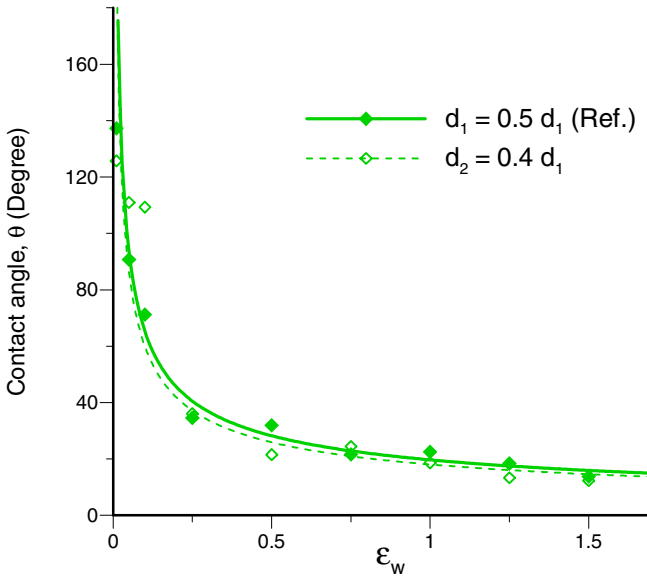

Fig. 5 Plot of contact angle as a function of the surface–liquid interaction energy parameter, illustrating the effect of the amount of droplet squeezing on contact angle.

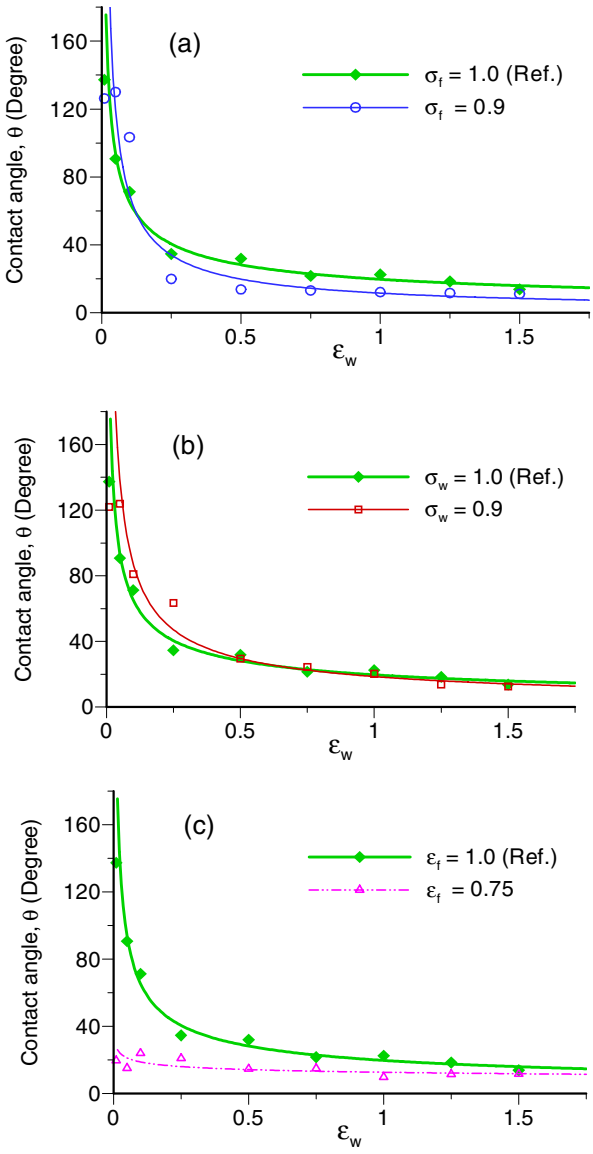

Fig. 6 Effect of liquid and solid molecular properties on contact angle plotted as a function of the surface–liquid interaction energy parameter; (a) effect of droplet molecular diameter (decrease in cohesive energy), (b) effect of surface porosity, (c) effect of liquid interatomic energy parameter (decrease in cohesive energy).

ters were kept unchanged. The effect of surface porosity on the contact angle is illustrated in Fig. 6b, which shows the variation of θ with ε_w for the two cases. For $\varepsilon_w < 0.5$, the contact angle increases as the surface porosity is increased (surface molecular diameter is decreased), while for $\varepsilon_w > 0.5$, the contact angle is relatively insensitive to the variation in surface porosity. Moreover, the transition from wettable to nonwettable surface occurs at slightly higher ε_w. This is an interesting result indicating that increasing the porosity makes a hydrophobic surface more hydrophobic (or a nonwettable surface more nonwettable). This may be expected since higher porosity reduces the fluid-surface interaction, and thus has an inverse effect on the surface wettability. This effect can be explained by considering the relative distance between the droplet and surface molecules. In this case, by lowering the size of the surface molecules, the surface–fluid interaction strength is lowered because of the increase in relative distance between surface–fluid molecules $r^*_{wf} = (r_{wf}/\sigma_{wf})$, where $\sigma_{wf} = (\sigma_w + \sigma_f)/2$, making the adhesive force weaker, while the

fluid cohesive force remains essentially constant. It is also important to note that the present simulation model can be used to examine the effect of surface roughness (i.e., by varying σ_w and other surface characteristics such as topology) on wettability. For instance, our results indicate that decreasing σ_w effectively increases the surface roughness, and this increases the hydrophobicity in the nonwettable region, which is consistent with the results of previous studies [36]. This aspect will be examined in a subsequent investigation.

Effect of Liquid Interatomic Interaction Energy (ε_f)

In this set of simulations, the effect of the interaction energy of the liquid atoms (ε_f) on the wetting behavior was studied. Figure 6c presents the variation of contact angle with ε_w for ε_f = 0.75 and 1.0. The results indicate a strong influence of ε_f on the surface wetting characteristics. This is primarily because the interaction energy between the droplet atoms is reduced by 25% from its reference value, while the liquid–surface interaction energy decreases by only 13%. As a result, we observe significant wetting for even low values of ε_w.

Wetting Dynamics and Comparison with Previous MD Results

In the preceding sections we have reported results from our simulations focusing on the wetting dynamics and the effects of various liquid and surface parameters on the contact angle. In this section we compare our results with available MD simulation results. The dynamic contact angle has been studied previously by Ruijter et al. [11]. We have also used our simulation to

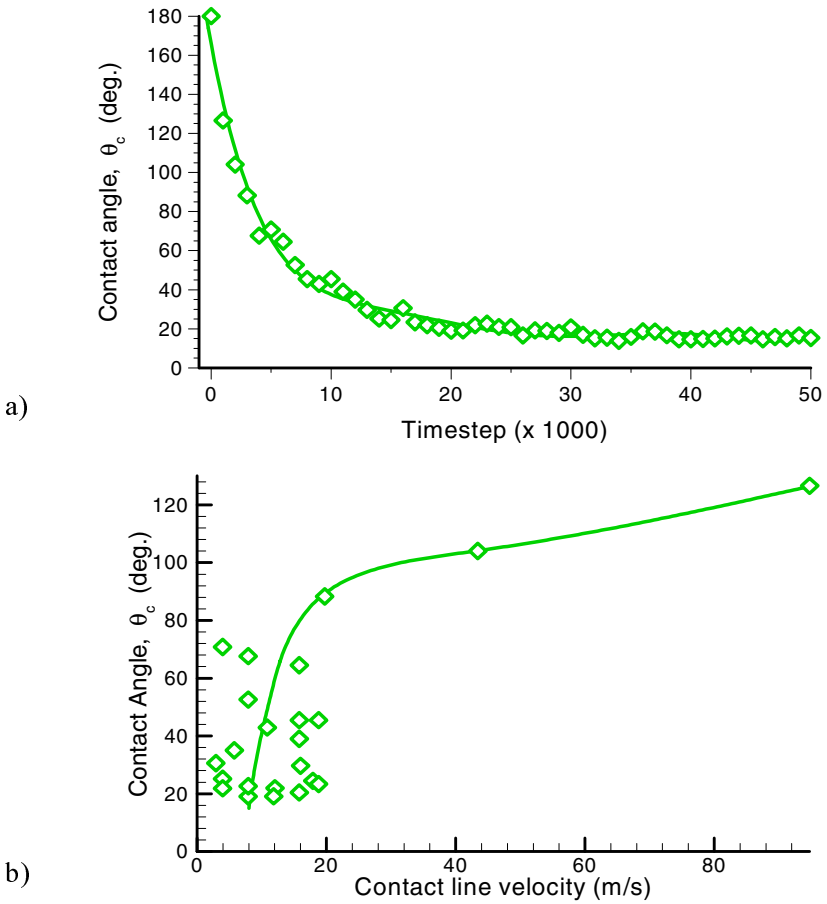

Fig. 7 (a) Temporal variation of the dynamic contact angle for a droplet spreading on a hydrophilic surface (reference case), and approach to equilibrium. (b) Variation of the dynamic contact angle with respect to the contact line velocity for the same case.

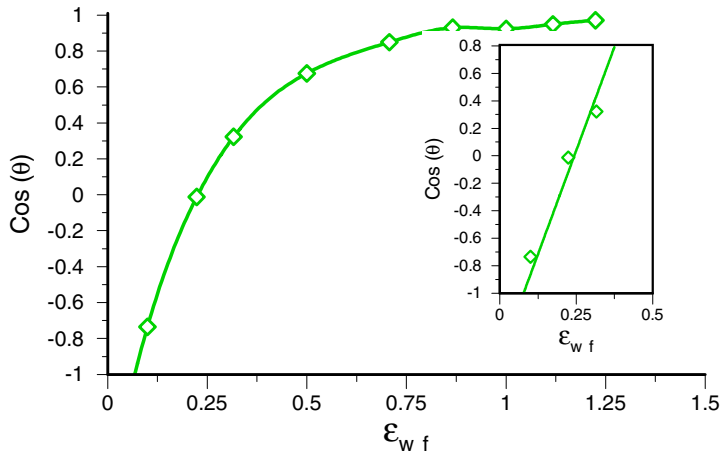

Fig. 8 Effect of solid–liquid interaction energy on cosine of contact angle for the reference case. As indicated in the inset, there is a linear relationship between cos (θ) and ε_{wf} in the partially wetting regime.

study the temporal variation of contact angle as the simulation progresses. The results are presented in Fig. 7a, which shows a rapid initial decrease in the contact angle within the first 10,000 steps, and then a more gradual approach to equilibrium in the next 10,000 steps. Over the next 30,000 steps, we observe only expected thermal fluctuations. This behavior is consistent with previous observations and further demonstrates the increased efficiency of our scheme.

In many previous studies [27, 32, 37, 38], the wetting dynamics have been characterized by examining the variation of contact angle (θ) with contact line velocity (V_{CL}). We computed the contact line velocity in our simulation by calculating the wetting diameter as a function of time. Figure 7b presents the variation of θ with V_{CL} for the case discussed in Fig. 7a. As the droplet is squeezed, its wetting diameter increases rapidly while it spreads on the surface. The contact line velocity is high in the beginning of the simulation. Subsequently, both the spread rate and the contact line velocity decrease rapidly. However, as the simulation proceeds further, the contact angle approaches equilibrium, and the rate of decrease in V_{CL} becomes small. In addition, as the contact line velocity approaches zero, i.e., near equilibrium, it exhibits significant fluctuations, as indicated in Fig. 7b. These fluctuations may be attributed to the pinning and depinning of the contact line as discussed in Ref. 32. Also, uncertainty in determining the contact diameter, while the system approaches equilibrium, contributes to fluctuations in the computed values of V_{CL}.

Ruitjer et al. [11] also examined the contact angle behavior in the partially wetting regime, characterized by relatively weak solid–liquid interactions compared to liquid–liquid interactions, and observed a linear relationship between cos (θ) and the strength of the liquid–solid interaction in this regime. In our simulations, the solid–liquid interaction is represented by ε_{wf}. The results of our simulation are plotted in Fig. 8, which also exhibits a linear relationship in the partially wetting regime (ε_{wf} = 0.075–0.375), as indicated in the inset of this figure. However, as solid–liquid interactions become stronger, the relationship becomes nonlinear, and ultimately cos (θ) approaches a value of unity corresponding to a completely wettable surface. This confirms that the solid–vapor and liquid–vapor interfacial tensions are independent of the solid–liquid interactions, as they should be, thus further validating our simulations.

CONCLUSIONS

We have reported MD simulations of the wetting phenomenon associated with nanodroplets. The dynamics of forced spreading of a droplet on a surface have been examined by squeezing an in-

itially spherical droplet between two moving surfaces. A new efficient algorithm has been developed to track the liquid-gas interface and the contact angle based on the computed density profiles. The algorithm has been shown to reproduce the entire wettability regime (θ ranging from 0 to 180 deg). Simulations have been carried out to investigate the effects of various molecular parameters on the wetting phenomena and contact angle. The parameters include the interaction energy of surface and liquid atoms, surface porosity, and the droplet molecular diameter.

Results indicate a highly nonlinear relationship between the contact angle and the surface-liquid interaction energy parameters. The wetting characteristics are also strongly influenced by the interaction parameters of droplet atoms. As the droplet molecular diameter is reduced, the surface wettability is enhanced in the hydrophilic (wettable) regime, while there is little effect in the nonwettable regime. The surface porosity has a relatively minor effect on the contact angle in the wettable regime, but has noticeable influence in the nonwettable regime, i.e., when the surface-liquid interactions are weak. The present study clearly demonstrates that MD simulations can be used quite effectively to investigate the wetting phenomena under forced spreading, and for characterizing the effects of surface tension and other macroscopic properties on wetting characteristics. Simulations using a relatively small number of atoms (on the order of the 10^4) demonstrated properties similar to the corresponding wetting phenomena on hydrophilic and hydrophobic surfaces. Results for the changes of fluid interfaces were also consistent with experimental observations and macroscopic theory.

REFERENCES

1. T. Werder, J. H. Walther, R. L. Jaffe, T. Halicioglu, F. Noca, and P. Koumoutsakos, Molecular Dynamics Simulation of Contact Angle of Water Droplets in Carbon Nanotubes, *Nano Lett.*, vol. 1, no. 12, pp. 697–702, 2001.
2. T. Young, An Essay on the Cohesion of Fluids, *Philos. Trans. R. Soc. Lond.*, vol. 95, pp. 65–87, 1805.
3. J. Hautman and L. M. Klein, Microscopic Wetting Phenomena, *Phys. Rev. Lett.*, vol. 67, no. 13, pp. 1763–1766, 1991.
4. P. S. Laplace, Suppleement à la Theorie de L'action Capillaire/de Laplace, Paris, 1807.
5. W. Zisman, Contact Angle, Wettability and Adhesion, *Adv. Chem. Series*, *Am. Chem. Soc.*, vol. 43, pp. 1–21, 1964.
6. F. M. Fowkes, Ed., Contact Angle, Wettability and Adhesion, *Adv. Chem. Series*, *Am. Chem. Soc.*, Washington D.C., vol. 43, pp. 1–21, 1964.
7. J. F. Padday, *Wetting Spreading and Adhesion*, Academic Press, New York, 1978.
8. C. Huh and L. E. Scriven, Hydrodynamic Model of Steady Movement of a Solid/Liquid/Fluid Contact Line, *J. Colloid Interface Sci.*, vol. 35, pp. 85–101, 1971.
9. F. Heslot, A. M. Cazabat, P. Levinson, and N. Fraysse, Experiment on Wetting on the Scale of Nanometers: Influence of the Surface Energy, *Phys. Rev. Lett.*, vol. 65, pp. 599–602, 1990.
10. S. Sikalo, H. D. Wilhelm, I. V. Roisman, S. Jakirlic, and C. Tropea, Dynamic Contact Angle of Spreading Droplets: Experiments and Simulations, *Phys. Fluids*, vol. 17, no. 6, pp. 1–13, 2005.
11. M. J. de Ruijter, T. D. Blake, and J. De Coninck, Dynamic Wetting Studied by Molecular Modeling Simulations of Droplet Spreading, *Langmuir*, vol. 15, pp. 7836–7847, 1999.
12. E. Cheng and C. Ebner, Dynamics of Liquid-Droplet Spreading: A Monte Carlo Study, *Phys. Rev. B*, vol. 47, no. 20, pp. 13808–13811, 1993.
13. P. A. Thompson, Simulation of Contact Line Motion: Slip and the Dynamic Contact Angle, *Phys. Rev. Lett.*, vol. 63, no. 7, pp. 766–769, 1989.
14. J. Koplik, J. R. Banavar, and J. F. Willemsen, Molecular Dynamics of Poiseuille Flow and Moving Contact Lines, *Phys. Rev. Lett.*, vol. 60, no. 13, pp. 1282–1285, 1988.
15. J. Fukai, Y. Shiiba, T. Yamamoto, and O. Miyatake, Wetting Effect on the Spreading of a Liquid Droplet Colliding with a Flat Surface: Experiment and Modeling, *Phys. Fluids*, vol. 7, no. 2, pp. 236–247, 1995.
16. J. F. Joanny and P. G. de Gennes, A Model for Contact Angle Hysterisis, *J. Chem. Phys.*, vol. 81, no. 1, pp. 552–562, 1984.
17. B. Muller, M. Riedel, R. Michel, S. M. De Paul, R. Hofer, D. Heger, and D. Grutzmacher, *J. Vac. Sci. Technol., B.*, vol. 19, no. 5, pp. 1715–1720, 2001.
18. J. W. Cahn, Critical Point Wetting, *J. Chem. Phys.*, vol. 66, pp. 3667–36727, 1977.
19. P. Lenz and R. Lipowsky, Morphological Transitions of Wetting Layers on Structured Surfaces, *Phys. Rev. Lett.*, vol. 80, no. 9, pp. 1920–1923, 1998.
20. M. J. P. Nijmeijer, C. Bruin, and A. F. Bakker, Wetting and Drying of an Inert Wall by a Fluid in a Molecular-Dynamics Simulation, *Phys. Rev.*

A, vol. 42, no. 10, pp. 6052–6059, 1990.
21. S. Maruyama, T. Kurashige, S. Matsomoto, Y. Yamaguchi, and T. Kimura, Liquid Droplet in Contact with a Solid Surface, *Micro. Thermophys. Eng.*, vol. 2, pp. 49–62, 1998.
22. J. Klier, P. Stefanyi, and A. F. G. Wyatt, Contact Angle of Liquid ^{4}He on a Cs Surface, *Phys. Rev. Lett.*, vol. 75, no. 20, pp. 3709–3712, 1995.
23. H. J. J. Verheijen and M. W. J. Prins, Contact Angles and Wetting Velocity Measured Electrically, *Rev. Sci. Instrum.*, vol. 70, no. 9, pp. 3668–3673, 1999.
24. C. F. Fan and T. Cagin, Wetting of Crystalline Polymer Surfaces: A Molecular Dynamics Simulation, *J. Chem. Phys.*, vol. 103, no. 20, pp. 9053–9061, 1995.
25. R. G. Cox, Inertial and Viscous Effects on Dynamic Contact Angles, *J. Fluid Mech.*, vol. 357, pp. 249–278, 1998.
26. T. D. Blake and J. M. Haynes, Kinetics of Liquid/Liquid Displacements. *J. Colloid Interface Sci.*, vol. 30, pp. 421–423, 1969.
27. I. S. Bayer and C. M. Megaridis, Contact Angle Dynamics in Droplets Impacting on Flat Surfaces with Different Wetting Characteristics, *J. Fluid Mech.*, vol. 558, pp. 415–449, 2006.
28. B. F. Bathel, N. Stephen, L. Johnson, A. Ratner, and M. Huisenga, Prediction of Postcontact Parameters of Fluid Droplet Impact on a Smooth Surface, *AIAA J.*, vol. 45-7, pp. 1725–1733, 2007.
29. S. Chandra, and C. T. Avedisian, On the Collision of a Droplet with a Solid Surface, *Proc. R. Soc. London: Math. Phys. Sci.*, vol. 432, no. 1884, pp. 13–41, 1991.
30. M. Pasandideh-Fard, Y. M. Qiao, S. Chandra, and J. Mostaghimi, Capillary Effects During Droplet Impact on a Solid Surface, *Phys. Fluids*, vol. 8, no. 3, pp. 650–659, 1996.
31. M. Pasandideh-Fard, S. Chandra, and J. Mostaghimi, A Three-Dimensional Model of Droplet Impact and Solidification, *Int. J. Heat Mass Transfer*, vol. 45, pp. 2229–2242, 2002.
32. T. D. Blake, The Physics of Moving Wetting Lines, *J. Colloid Interface Sci.*, vol. 299, pp. 1–13, 2006.
33. L. Consolini, S. K. Aggarwal, and S. Murad, A Molecular Dynamics Simulation of Droplet Evaporation, *Int. J. Heat Mass Transfer*, vol. 46, pp. 3179–3188, 2003.
34. P. G. De Gennes, F. Brochard-Wyart, and D. Quere, *Capillary and Wetting Phenomena*, Springer, New York, 2002.
35. D. P. Woodruff, *The Solid Liquid Interface*, Cambridge University Press, Cambridge, England, 1973.
36. A. Lafuma and D. Quere, Superhydrophobic States, *Nat. Mater.*, vol. 2, no. 7, pp. 457–460, 2003.
37. T. D. Blake, in *Wettability*, J. C. Berg (Ed.), Dekker, New York, pp. 251–310, 1993.
38. E. B. Dussan V., On the Spreading of Liquid on Solid Surface: Static and Dynamic Contact Angle, *Annu. Rev. Fluid Mech.*, vol. 11, pp. 371–400, 1979.